Radiation Protection Dosimetry (year), Vol. 0, No. 0, pp. 0–0
DOI: 10.1093/rpd/nc0000

MODELLING DNA DAMAGE BY PHOTONS AND LIGHT IONS OVER ENERGY RANGES USED IN MEDICAL APPLICATIONS

W. Friedland[1,*], P. Kundrát[1], E. Schmitt[1], J. Becker[1], W. Li[1]
[1]Institute of Radiation Protection, Helmholtz Zentrum München – German Research Center for Environmental Health, Neuherberg, Germany

Received month date year, amended month date year, accepted month date year

Comprehensive track structure-based simulations of DNA damage induced in human cells by photons (5 keV – 1.3 MeV) and light ions (0.25 – 512 MeV/u) were performed with PARTRAC. DNA strand breaks, double-strand breaks, and their clustering were scored. Effective LET values were established for photons that provide LET-dependent damage yields in agreement with the data for ions. The resulting database captures the variations of biological effectiveness with radiation quality. In particular, it can help compare the effectiveness of conventional radiotherapy using photon beams with techniques relying on proton or ion beams.

INTRODUCTION

PARTRAC[(1)] is a biophysical simulation tool for modelling radiation effects on subcellular and cellular scales. It consists of mutually interlinked modules that reflect the mechanisms underlying the biological effects of ionizing radiation. The tool starts from a cross section database that is used to model the stochastic nature of individual energy deposition events. Tracks of photons, electrons, protons and light ions can be simulated over wide energy ranges that occur naturally or in medical or technical applications. Following these simulations on radiation physics, the formation of reactive species, their diffusion and mutual reactions are modelled. Subsequently, the induction of damage to cellular DNA is simulated, taking into account both direct energy deposits and attacks of reactive species. The implemented multi-scale models of DNA and chromatin structures include DNA double-helical structure, wrapping around histones, and formation of chromatin fibres, loops, domains, and chromosome territories within the nucleus. In the next module, DNA damage response through non-homologous end joining of DNA double-strand breaks (DSB) is followed, explicitly considering both temporal and spatial aspects by modelling enzymatic processing and mobility of DNA termini. Correct rejoining, misrejoining and the formation of chromosome aberrations are simulated. Work in progress aims at extending PARTRAC to the endpoint of cell killing.

Recently, a comprehensive evaluation of DNA damage by light ions (H, He, C, N, O and Ne) has been undertaken from 256 MeV/u down to stopping[(2)]. Low-energy ion cross sections have been determined by a refined Barkas scaling approach[(2,3)], applicable down to about 10 keV/u. The simulations have shown that protons and He ions induce more DNA damage than heavier ions at the same linear energy transfer (LET). With increasing LET, DNA strand break (SB) yields are steadily decreasing, but due to their clustering the DSB yields increase up to saturation around 300 keV/μm. In addition, also individual DSB tend to cluster; DSB clusters peak around 500 keV/μm while DSB multiplicities per cluster continue to increase with LET. If the individual DSB in clusters are not resolved, i.e., isolated DSB and DSB clusters are scored as single DSB sites, the LET-dependent yields for C and heavier ions are uniquely peaking around 200 keV/μm with the same yield but about 10% below the yield for He.

The present work complements the previous analysis in several points: (i) The range of ion energies is extended to 512 MeV/u, since comparably high energies may be needed in radiotherapy with light ions. (ii) The gap between He and C ions is filled by including Li, Be and B ions. (iii) The analysis is extended to diverse photon radiations, including monoenergetic photons and X-ray spectra. (iv) The impact on the resulting DNA damage is addressed of the size of the simulated region and the related deviations from electronic equilibrium conditions.

METHODS

Simulation setup and DNA damage classification

The previous analysis[(2)] of DNA damage induction by ^{1}H, ^{4}He, ^{12}C, ^{14}N, ^{16}O, and ^{20}Ne ions with starting energies of 0.25, 0.5, 1, 2, 4, 8, 16, 32, 64, 128, and 256 MeV/u was extended to 512 MeV/u and complemented by data for ^{7}Li, ^{9}Be and ^{11}B ions, using the same setup as previously. The ions started from a rotating circular source of 80 μm² tangential to a spherical model of a human lymphocyte nucleus (10 μm diameter), which included the standard DNA and chromatin structure[(1)]. The simulation region (‘world

*Corresponding author: friedland@helmholtz-muenchen.de

© The author (year). Published by Oxford University Press; all rights reserved

region') consisted of a sphere of 14.2 µm diameter around the centre of the nucleus. Secondary electrons were followed only within this world volume. This does not provide electronic equilibrium as given when the ions penetrate macroscopic distances through biological material before entering the cell nucleus. To determine the contribution of electrons formed outside the world volume to nuclear dose and DNA damage, in dedicated simulations the ion source was placed up to 10 mm away from the nucleus, and backscattered electrons from up to 0.3 mm behind the cell were included, too. The maximum source distance (10 mm) was chosen so as to guarantee full electronic equilibrium conditions: the continuous slowing-down approximation (csda) range of the most energetic electrons (about 1.4 MeV) produced by 512 MeV/u ions is about 7 mm.

The photon radiations considered in this work include monoenergetic 5 and 10 keV photons, a 30 kVp mammography X-ray spectrum (W anode, 0.05 mm Rh filtration, 18.9 keV mean energy), low filtered (3.9 mm Al + 0.5 mm Be) X-ray spectra[4] with 50, 60, 80, 100, 150, 200 and 250 kVp (mean energies ranging from 33.8 up to 81.3 keV), and γ-rays from ^{137}Cs (662 keV) and ^{60}Co (mean energy 1255 keV) decays. Simulations on DNA damage by photons used the same target configuration as for ions. A cube of 10 µm side length surrounding the target sphere was adopted as world region in which photons were started from random positions in random directions. To save computation time, interactions of photons and secondary electrons were mirrored into the world region; this also ensured complete equilibrium of secondary electrons.

Breaks on both DNA strands within 10 bp (base pairs) were scored as DSB. Multiple DSB not separated by at least 25 bp were classified as a single cluster. An isolated DSB or a cluster were both scored as DSB sites.

Interaction cross sections

Interaction cross sections for individual charge states of H (hydrogen atoms and protons) and He (He^0, He^+, He^{2+}) are implemented in PARTRAC[1]. Cross sections for ions heavier than He, including Li, Be and B newly presented here, were determined by scaling by the squared effective charge Z_{eff}^2 the cross sections for H (energy-dependent mixture of neutral hydrogen atoms and protons) at the same energy per nucleon, as described in detail in Refs.[2,3]. This scaling can be used at energies as low as 10 keV/u; for lower energies, nuclear reactions can no longer be neglected. For specific energies above 1 MeV/u, the scaling approaches the usual Barkas method.

For photons, interaction cross sections were taken from the EPDL database, as done standardly in PARTRAC[1]. Explicitly considered were the following processes: coherent scattering, photoelectric effect, Compton scattering, Auger electron and fluorescence photon emission. The additivity rule and density scaling were used to determine photon interactions based on atomic cross sections and the elemental composition of the cell nucleus.

Secondary and higher-order electrons liberated by the primary ions or photons (or lower-order electrons) were processed by the electron transport module[1]. Elastic scattering, five excitations and five ionization levels were considered for liquid water, taken as a surrogate for biological material.

Characterizing radiation quality by LET

LET is commonly used in radiation biology as a descriptor of radiation quality. For ions, LET values were determined by the relation between dose absorbed within the cell nucleus and the particle fluence; for very low-energy ions whose ranges are smaller than the diameter of the cell nucleus, only its irradiated part was considered. For Li, Be and B ions, LET ranged from 2.0, 3.5 and 5.5 keV/µm at 512 MeV/u to 380, 590 and 780 keV/µm at 0.5 MeV/u, respectively.

Photon radiation quality is typically represented by microdosimetric quantities, in particular by dose- or fluence-mean lineal energy (y_D, y_F). These quantities can be used for ions as well; they largely vary with target sizes < 100 nm, but approach LET for targets > 100 nm[5,6]. In this work, y_D and y_F in 10, 100 and 1000 nm-diameter spheres were determined for photons. Alternatively, similarly to the LET calculation for ions, energy deposits by photons and their secondary electrons were scored within 100nm slabs placed at the centre of the cell nucleus parallel to the source. Then they were divided by the number of photons that interacted there (in analogy to the fluence of ions) and the slab thickness. In the following, the resulting quantity is termed interacting fluence-based LET_γ.

RESULTS

Values of dose- or fluence-mean lineal energy and interacting fluence-based LET_γ are for the considered photon radiation qualities plotted in Figure 1. The dose-mean values are larger than the fluence-mean ones, and both y_D and y_F increase with decreasing target size, as is well known in microdosimetry[5,6]. LET_γ increases also with decreasing slab thickness. In general, y_D, y_F and LET_γ increase with decreasing mean photon energy; the variation between ^{60}Co γ-rays and 5 keV X-rays is by factors of 2 and 12 for y_D in 100nm-sized targets and LET_γ, respectively. At MeV energies, LET_γ equals y_F. Finer structures can be identified for mean photon energies between 30 and 70 keV, due to the transition from the dominance of the photoelectric effect to Compton scattering; however, the resulting variations are small compared to the overall trend in the whole studied region.

As illustrated in Figure 2, photon-induced DNA damage in dependence on LET_γ is consistent with that

induced by ions in dependence on their LET, showing linear increase of DSB sites and DSB clusters with LET. LET_γ thus provides a measure of radiation quality analogous to the LET. The variation in y_D with mean photon energy (Figure 1) is too low to match the LET-dependence for ions (Figure 2). Anyway, in general, the biological effectiveness of 5 keV–1.3 MeV photons in terms of DNA damage induction is comparable to that of low-LET (i.e., high-energy) protons and ions.

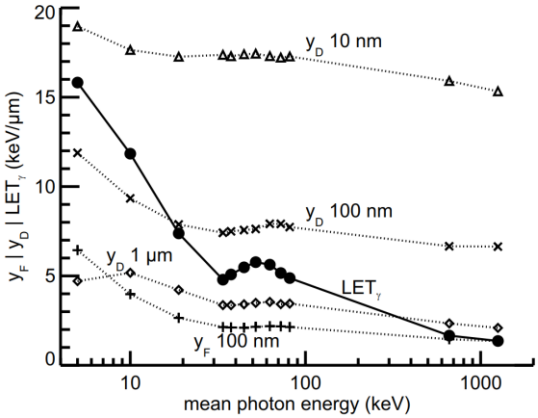

Figure 1. Dose-mean lineal energy y_D in 10, 100, or 1000nm-diameter target spheres, fluence-mean lineal energy y_F in 100nm-diameter spheres, and interacting fluence-based LET_γ in 100nm-thick slab, in dependence on mean photon energy. Symbols depict the simulation results; lines connect them to guide the eyes only.

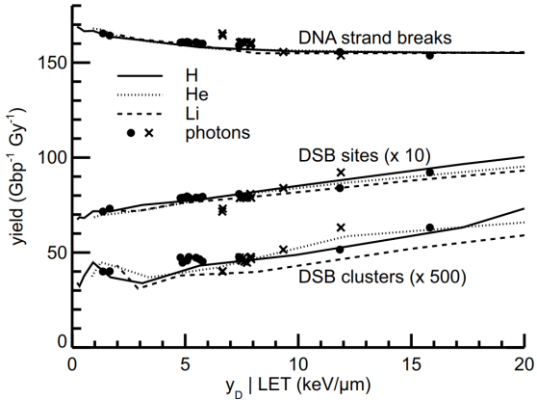

Figure 2. DNA damage yields after sparsely ionizing radiation in dependence on LET for ions (lines) or its analogues for photons (symbols), dose-mean lineal energy y_D in 100nm-diameter target sphere (crosses) and interacting fluence-based LET_γ in 100nm-thick slab (circles). Differences between ions are not significant; standard errors for DNA strand breaks, DSB sites and DSB clusters are 0.3–1.2%, 1–2% and 7–17%, respectively (not plotted).

The variations in biological effectiveness over large ranges of LET are shown in Figs. 3 and 4; for X-ray spectra, only 30 and 100 kVp data are included. Low-LET radiation induces about 7–9 DSB sites per Gbp per Gy (Figure 3), i.e. 42–54 DSB sites per cell per Gy. These figures about double for most effective radiations, namely H ions around 60 keV/µm or He ions around 200 keV/µm. Heavier ions possess slightly reduced maxima in the induction of DSB sites at 200–300 keV/µm. At higher LET values, the yields of DSB sites drop considerably.

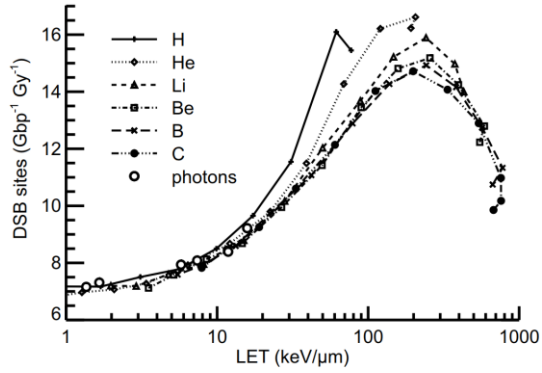

Figure 3. Ion- and photon-induced DSB sites in dependence on LET (or LET_γ for photons). Symbols depict the simulations, lines are to guide the eyes only.

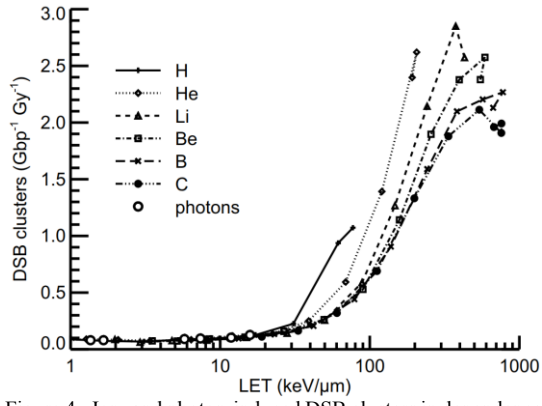

Figure 4. Ion- and photon-induced DSB clusters in dependence on LET (or LET_γ for photons). Symbols depict the simulations, lines are to guide the eyes only.

In Figure 4, corresponding results are presented for DSB clusters. H and He ions are more effective than heavier ions at the same LET. Compared with DSB sites, the maximum in effectiveness is shifted towards higher LET and the drop in effectiveness at the highest LET values is lower.

All the above results for ions were obtained with the source tangential to the cell nucleus (i.e. at 5µm distance from its centre), in which electronic equilibrium conditions were not fulfilled, especially for high-energy ions. Figure 5 shows the effect of equilibrium build-up on dose absorbed in the nucleus, SB and DSB yields, addressed in dedicated simulations with varied distance

of the source from the nucleus. To include the contributions from backscattered electrons, the simulation region was extended to 0.3 mm behind the centre of the nucleus. Considering the backscattered electrons leads to dose and DNA damage enhancements of up to 7% (left-most points in Figure 5). With increasing source distance from the nucleus, i.e. as the electronic equilibrium gradually builds up, doses to cell nucleus as well as the induction of SB and DSB increase further. The increase in dose for 512 MeV/u (7.9 keV/µm) C ions reaches 23%, and in SB yields 25%, compared to the standard setup. For 256 MeV (0.32 keV/µm) protons, the build-up factors are similar for dose, SB and DSB yields and culminate at 19%. High-LET Ne ions (32 MeV/u, 169 keV/µm) can produce secondary electrons with considerably smaller energies only, and hence the build-up is complete in 0.1 mm distance; dose and SB increase by up to 8%, DSB by 4%.

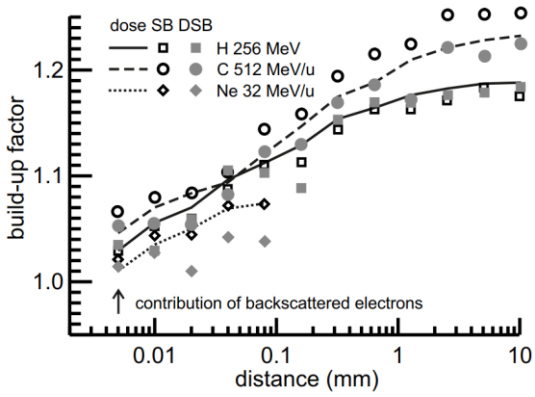

Figure 5. Build-up of dose, SB and DSB induction due to secondary electrons, assessed by increasing the distance of the source from the centre of the cell nucleus. Backscattering from up to 0.3 mm has been included, too. Build-up factors depict the results relative to the standard setup.

DISCUSSION AND CONCLUSION

The previous analysis of DNA damage induced by 0.25 – 256MeV/u ions has been extended to 512 MeV/u, complemented by Li, Be and B ions, and compared to simulation results for photons. The results support the previously reported LET-dependences[2].

Under electronic equilibrium condition the SB induction can be ~25% higher than in the build-up region. However, similar increase in the absorbed doses limits the enhancement of SB yields (per unit dose) to ~2%. DSB yields for fast ions are essentially unchanged but for ions with higher LET they may decrease by ~4% due to the additional irradiation by fast electrons with low biological effectiveness.

The interacting fluence-based LET_γ has been defined for photons in analogy to LET that is commonly used to characterize the biological effectiveness of ion beams. Both provide a consistent means of characterizing radiation quality with respect to DNA damage induction. In this context, LET_γ is superior to dose-mean lineal energy; the latter exhibits variations that are too low to explain the differences in damage induction by photons of diverse energies in agreement with the LET-dependent ion data. Yields of SB, DSB sites and DSB clusters correspond for ^{60}Co and ^{137}Cs γ-rays to 1-2 keV/µm ions. The 50-250 kVp X-ray spectra yield ~10% more DSB sites and 12% more DSB clusters than ^{60}Co or ^{137}Cs γ-rays, matching to 4-8 keV/µm ions; no significant differences in DNA damage are seen among these spectra.

In summary, the present results complement the previously published database of track-structure simulations on radiation-induced damage to DNA. The new results for light ions and for photons agree with previously reported LET-dependences. The results quantify initial DNA damage by diverse radiation types over wide energy ranges relevant in medical applications, and as such will be helpful in modelling their biological effectiveness.

FUNDING

Supported by EURATOM (FP7/2007-2011) under grant agreement no. 249689 (DoReMi).

REFERENCES

1. Friedland, W., Dingfelder, M., Kundrát, P., Jacob, P. *Track structures, DNA targets and radiation effects in the biophysical Monte Carlo simulation code PARTRAC.* Mutat. Res. **711**, 28-40 (2011).
2. Friedland, W., Schmitt, E., Kundrát, P., Dingfelder, M., Baiocco, G. and Ottolenghi, A. *Comprehensive track-structure based evaluation of DNA damage by light ions from radiotherapy-relevant energies down to stopping.* Sci. Rep. **7**, 45161 (2017).
3. Schmitt, E., Friedland, W., Kundrát, P., Dingfelder, M. and Ottolenghi, A. *Cross-section scaling for track structure simulations of low-energy ions in liquid water.* Radiat. Prot. Dosimetry **166**, 15-18 (2015).
4. Poludniowsky, G., Landry, G., DeBlois, F., Evans, M.P. and Verhaegen, F. *SpekCalc: a program to calculate photon spectra from tungsten anode x-ray tubes.* Phys. Med. Biol. 54, N433-N438 (2009)
5. Olko, P. *Microdosimetric modelling of physical and biological detectors.* Habilitation Thesis. Report 1914/D. Institute of Nuclear Physics, Kraków, Poland (2002). www.ifj.edu.pl/reports/2002.html
6. Lindborg, L., Hultqvist, M., Carlsson Tedgren, Å. and Nikjoo, H. *Lineal energy and radiation quality in radiation therapy: model calculations and comparison with experiment.* Phys. Med. Biol. **58**, 3089-3105 (2013).